

# Synthesis of Highly Active Doped Graphitic Carbon Nitride using Acid-Functionalized Precursors for Efficient Adsorption and Photodegradation of Endocrine-Disrupting Compounds

Adeem Ghaffar Rana,<sup>[a, b]</sup> Mian Zahid Hussain,<sup>[c]</sup> Nikki Hammond,<sup>[a]</sup> Simon Vlad Luca,<sup>[a]</sup> Roland A. Fischer,<sup>[c]</sup> and Mirjana Minceva<sup>\*[a]</sup>

A highly active non-metallic doped bulk graphitic carbon nitride ( $g\text{-C}_3\text{N}_4$ ) was synthesized via acid-functionalized melamine decomposition. Specifically, melamine was treated with acetic acid, sulfuric acid, and phosphoric acid to obtain oxygen, sulfur, and phosphorus-doped  $g\text{-C}_3\text{N}_4$  derivatives. Sulfur-doped  $g\text{-C}_3\text{N}_4$  exhibited remarkable photocatalytic activity to degrade two environmentally harmful hormones,  $17\beta$ -estradiol, and  $17\alpha$ -ethinylestradiol, due to its narrow energy bandgap and high surface area. The hormones were removed entirely in 30–

45 min by adsorption in the dark, followed by photodegradation under visible light (430 nm). Furthermore, the pseudo-second-order kinetic model fitted the adsorption kinetics well, and photocatalytic degradation followed the exponential decay model. LC–MS identified the intermediate products for the photodegradation of  $17\beta$ -estradiol (E2). This study provides a simple one-step method to synthesize highly reactive metal-free doped bulk  $g\text{-C}_3\text{N}_4$  photocatalysts to remove harmful water pollutants.

## Introduction

Pollution caused by endocrine-disrupting compounds (EDCs) is a persistent challenge in water treatment.<sup>[1]</sup> EDCs pose a health hazard to humans and animals and are a growing environmental concern.<sup>[2]</sup> These compounds can interfere with the hormone balance in humans and animals and adversely affect reproduction, sexual development, stress response, and the body's overall chemical equilibrium.<sup>[3]</sup> Exposure to EDCs can even lead to several human cancers.<sup>[4]</sup> EDCs disrupt the normal endocrine function by interacting with hormone receptors and mimicking natural estrogens' physiological function.<sup>[5]</sup> Among EDCs, which include both natural and synthetic compounds,<sup>[3]</sup>  $17\beta$ -estradiol (E2) and  $17\alpha$ -ethinylestradiol (EE2) are the most harmful and persistent natural estrogens.<sup>[4]</sup> E2 is a natural

hormone in women and is associated with the reproductive system; on the other hand, EE2 is a synthetic hormone produced from natural E2 and used as the active ingredient in some oral contraceptives. Even at low concentrations (ng/L), E2 and EE2 have a solid estrogenic effect.<sup>[1]</sup> E2 primarily enters the water systems via human and animal urine; however, the intake of products such as birth control pharmaceuticals and other hormonal products used in the dairy industry can cause an increase in its prevalence as a pollutant in water.<sup>[6]</sup> E2 is resistant to typical sewage treatment procedures and frequently gets released back into the water from where it can enter drinking and surface water.<sup>[7]</sup> Given the threats that E2 and EE2 pose to human health,<sup>[3]</sup> a need exists to develop effective treatment processes to remove these compounds from water systems.

Advanced oxidation processes (AOPs) are alternative solutions to removing organic pollutants like E2 from aqueous media.<sup>[4]</sup> Although AOP systems rely on various reaction means and methods, they all share the common characteristic of producing  $\cdot\text{OH}$  radicals. The reactivity of  $\cdot\text{OH}$  radicals toward organic molecules, combined with their limited selectivity, renders them beneficial oxidants for wastewater treatment.<sup>[8]</sup> Indeed,  $\cdot\text{OH}$  radicals have been observed to play a vital role in removing and degrading toxic wastewater contaminants into benign species.<sup>[9]</sup> Among the various AOP processes, photocatalysis is one of the promising approaches to wastewater treatment, as it is cost-effective, highly efficient, and exhibits low toxicity.<sup>[2]</sup>

The reaction kinetics of photocatalysis is affected by multiple factors, including the catalyst's appropriate energy bandgap and surface properties, the incident light's wavelength, and the target compound's chemical properties.<sup>[1]</sup> Although a wide variety of catalytic materials exist that can be used in photo-

[a] A. Ghaffar Rana, N. Hammond, Dr. S. Vlad Luca, Prof. Dr. M. Minceva  
Biothermodynamics, TUM School of Life Sciences  
Technical University of Munich  
Maximus-von-Imhof-Forum 2,  
Freising 85354, Germany  
E-mail: Mirjana.minceva@tum.de

[b] A. Ghaffar Rana  
Department of Chemical, Polymer, and Composite Materials Engineering  
University of Engineering and Technology (UET)  
Lahore 39161, Pakistan

[c] Dr. M. Zahid Hussain, Prof. Dr. R. A. Fischer  
Department of Chemistry and Catalysis Research Center  
Technical University of Munich  
Garching 85748, Germany

Supporting information for this article is available on the WWW under <https://doi.org/10.1002/slct.202201909>

© 2022 The Authors. ChemistrySelect published by Wiley-VCH GmbH. This is an open access article under the terms of the Creative Commons Attribution License, which permits use, distribution and reproduction in any medium, provided the original work is properly cited.

catalysis, graphitic carbon nitride ( $g\text{-C}_3\text{N}_4$ ) has emerged as one of the most promising materials for photocatalytic applications in both environmental and energy-producing processes.<sup>[10]</sup>  $g\text{-C}_3\text{N}_4$  is a non-toxic polymeric semiconductor exhibiting high chemical and thermal stability.<sup>[11]</sup> This semiconductor can easily be synthesized from compounds such as melamine and urea via the thermal decomposition of nitrogen-rich precursors under appropriate reaction conditions. The main drawback of  $g\text{-C}_3\text{N}_4$  is its limited photocatalytic activity resulting from its low surface area.<sup>[11]</sup> Some techniques like exfoliation improve the surface area and performance but need additional heat. Metal doping has become a popular approach to improving the photocatalytic performance of  $g\text{-C}_3\text{N}_4$ ,<sup>[10]</sup> however, using metals can be costly and environmentally unfriendly, and it may cause the catalyst to become toxic. Therefore, developing alternative strategies for increasing the photocatalytic activity of  $g\text{-C}_3\text{N}_4$  is a crucial research goal.

This study aims to enhance the activity of  $g\text{-C}_3\text{N}_4$  in removing harmful estrogenic compounds from water systems without adding metals to the catalytic system. To achieve this goal, melamine was functionalized with non-metallic elements such as sulfur (S), oxygen (O), and phosphorus (P) to obtain the synthesized doped  $g\text{-C}_3\text{N}_4$  species. The activity of the doped catalysts was tested for degradation of  $17\beta$ -estradiol and  $17\alpha$ -ethinylestradiol in an aqueous solution using adsorption in dark and photodegradation in a stirred glass reactor under irradiation with an immersion LED lamp. The extent of EDC photodegradation was determined by analyzing the concentration of the hormones in the water solution at regular time intervals using high-performance liquid chromatography (HPLC) technology.

## Results and Discussion

### Photocatalyst characterization

The crystalline structures of the undoped  $g\text{-C}_3\text{N}_4$  (BCN) and S, O, and P doped  $g\text{-C}_3\text{N}_4$  (SBCN, OBCN, and PBCN) samples synthesized after decomposition of acid-treated melamine

were determined based on the powder X-ray diffraction (PXRD) patterns reported in Figure 1a. BCN, OBCN, and SBCN catalysts exhibited the characteristic peaks of  $g\text{-C}_3\text{N}_4$  at about  $2\theta$  of  $27.3^\circ$  and  $2\theta$  of  $13.1^\circ$ . From the (002) plane, the high-intensity peak is due to the typical interlayer stacking of conjugated aromatic systems like  $g\text{-C}_3\text{N}_4$ . Moreover, a minor peak due to the (100) plane is ascribed to repeated units of tri-s-triazine.<sup>[11–12]</sup> The PXRD peak intensities of BCN and OBCN are almost the same, while in the case of SBCN, the peak intensity is slightly lower. Although no peaks due to phosphorus were observed in PBCN, the intensity of the  $g\text{-C}_3\text{N}_4$  PXRD characteristic peaks has decreased, indicating the reduction in the crystallinity of this material. Indeed, the presence of large amounts of phosphorus in the catalyst can be assumed to cause an enhancement of layer spacing.<sup>[13]</sup> During the poly-condensation of acid-treated precursors, the loss of lattice C or N centers leads to a change in the crystalline structure, which inhibits the growth of  $g\text{-C}_3\text{N}_4$  crystals.<sup>[13–14]</sup> In addition, the PXRD patterns of PBCN comprised (see inset in Figure 1a) an extremely broad (002) peak, and the relative intensities of both peaks massively decreased compared to BCN. This broad peak is due to the significant phosphorus content, indicating that the growth of  $g\text{-C}_3\text{N}_4$  crystals is inhibited by introducing phosphoric acid.<sup>[14]</sup>

The FTIR spectra were recorded to determine the prepared samples' doping extent. The FTIR spectra of the doped and undoped  $g\text{-C}_3\text{N}_4$  samples are presented in Figure 1b. The peaks observed between  $1650$  and  $1242\text{ cm}^{-1}$  can be attributed to the stretching vibration modes of the C–N bond and the aromatic C=N heterocyclic species in repeated units of tri-s-triazine.<sup>[12,15]</sup> Additionally, the sharp peak appearing at  $813\text{ cm}^{-1}$  in the spectra of BCN, OBCN, and SBCN is due to the breathing mode of the s-triazine ring system. Still, this peak was almost absent in the FTIR spectrum of PBCN, which indicates that tri-s-triazine in this catalyst undergoes a drastic modification.

On the contrary, the broad-band visible in the  $3100\text{--}3500\text{ cm}^{-1}$  wavenumber range in the spectra of all four catalysts can be attributed to the vibration modes of the OH group from adsorbed water molecules and the stretching vibrations of N–H bonds from residual amino groups. In the

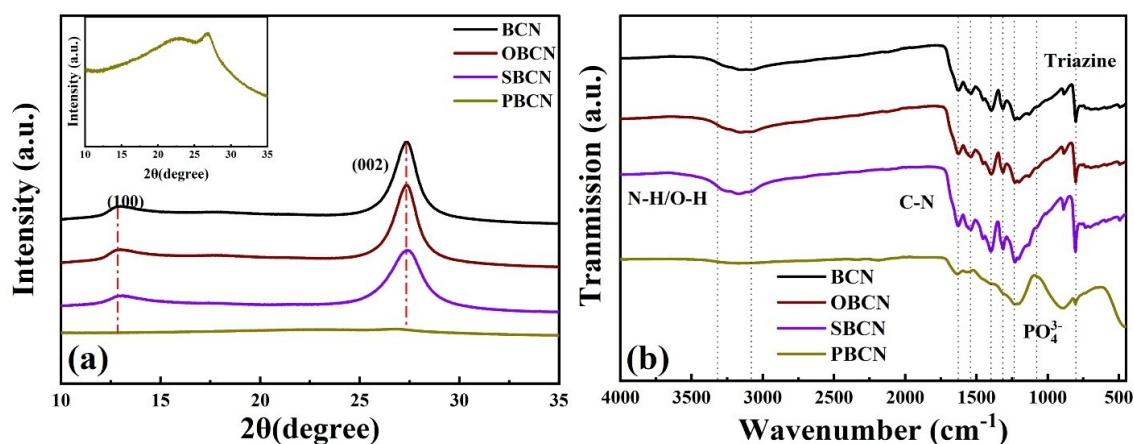


Figure 1. (a) PXRD and (b) FTIR spectra of BCN and doped OBCN, SBCN, and PBCN.

PBCN spectrum, a broad peak between 1250 and 800  $\text{cm}^{-1}$  was identified due to the vibration modes of  $\text{PO}_4^{3-}$  groups.<sup>[16]</sup> Also, the intensity of the spectra of PBCN is low compared to BCN. This observation can be ascribed to a modification in the chemical structure of tri-s-triazine due to the presence of P in the catalyst, and this result was in good agreement with PXRD data (Figure 1a). In the SBCN spectrum, no prominent peaks attributable to moieties containing S were observed, probably due to the low sulfur content in the structure of this species.<sup>[15]</sup> The BCN and OBCN have shown similar FTIR spectra. The results of the further characterization performed in this work are graphically presented only for the doped  $\text{g-C}_3\text{N}_4$  catalysts. The complete characterization results of undoped  $\text{g-C}_3\text{N}_4$  are presented in our previous work.<sup>[11]</sup>

The chemical composition of the OBCN, SBCN, and PBCN samples was investigated using X-ray photoelectron spectroscopy (XPS). Notable, the XPS elemental survey spectra of the samples (Figure S1) confirmed the presence of C, N, and O in all samples. The C/N ratio in PBCN is lower than in OBCN and SBCN; P in PBCN is 21.32 atomic % pointing to the possible reason behind the observed reduction in C and N contents in the sample. Remarkably, S present in SBCN is only 0.16 atomic %. This observation is because  $\text{CH}_3\text{COOH}$  and  $\text{H}_2\text{SO}_4$  were removed during the heating and sublimation of melamine. However, phosphorous is not entirely removed from the  $\text{g-C}_3\text{N}_4$  structure as  $\text{PO}_4^{3-}$  cannot be decomposed entirely at melamine's decomposition temperature (550  $^\circ\text{C}$ ).<sup>[17]</sup>

The C 1s and N 1s XPS spectra were recorded to investigate the interaction between C and N atoms. The deconvoluted C 1s XPS spectra of the doped samples (Figure 2a) exhibited two strong peaks appearing at 285 and 288 eV, which can be assigned to the standard (C–C) carbon bonds and  $\text{sp}^2$  hybridized carbon (N–C=N) in triazine rings.<sup>[11,18]</sup> Two low-intensity peaks observed at 286 and 289 eV can be assigned to the amino-functional groups (C–NH<sub>2</sub>) and the carboxyl group (O–C=O) bound to the surface of  $\text{g-C}_3\text{N}_4$ , respectively.<sup>[11,18a,19]</sup> In the case of PBCN, the intensities of C 1s peaks were substantially lower than their counterparts observed for SBCN and OBCN, which indicates that the C atoms might have been replaced by P atoms in the chemical structure of  $\text{g-C}_3\text{N}_4$ .<sup>[20]</sup> The deconvoluted N 1s spectra (Figure 2b) exhibited three prominent peaks at around 398.4, 400.2, and 401.2 eV for OBCN and SBCN with varying intensities. The strong peak at 397.8 eV corresponds to the triazine rings'  $\text{sp}^2$  hybridized nitrogen atom bound to carbon (C–N=C). The other two peaks of medium intensity appearing at 400.2 and 401.2 eV can be assigned to the presence of tertiary N in N–(C)<sub>3</sub> units and amino functional groups (NH<sub>2</sub> or NH), respectively.<sup>[11,18,20]</sup>

The O 1s spectrum of OBCN reported in Figure 2c includes peaks at 532.7 and 535.7 eV, corresponding to the O–C–N/C–O bonds and adsorbed moisture, respectively.<sup>[21]</sup> Notably, deconvolution of the S 2p spectrum of SBCN reported in Figure 2d indicated the presence of three peaks at 163.9, 165.1, and 168.9 eV. The peak at 163.9 eV can be assigned to the C–S bond formed due to the substitution of lattice nitrogen with

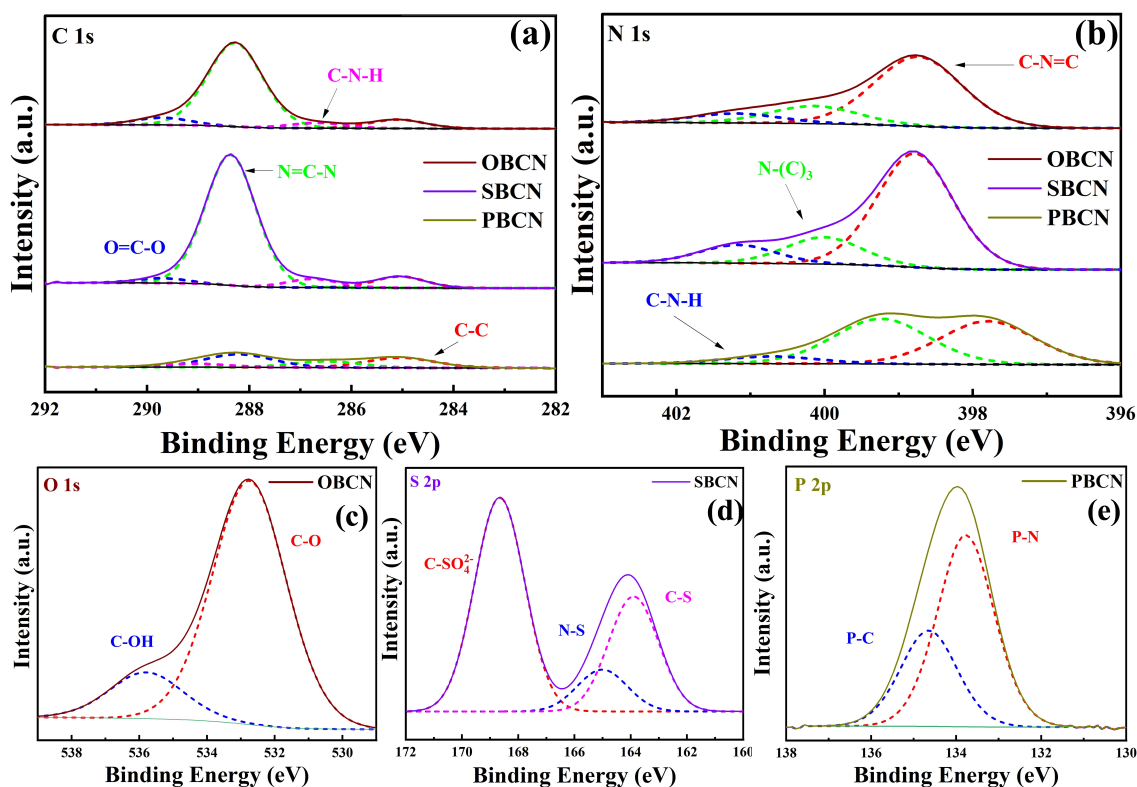


Figure 2. High resolution deconvoluted XPS spectra of (a) C 1s (b) N 1s (c) O 1s (d) S 2p, and (e) P 2p for catalysts OBCN, SBCN, and PBCN.

sulfur. The weakest peak was at 165.4 eV, which was regarded due to N–S bonds resulting from replacing lattice carbon with sulfur. The most substantial peak was centered at 169.3 eV, indicating that  $\text{SO}_4^{2-}$  was present in SBCN.<sup>[15,22]</sup> The P 2p spectrum of PBCN (reported in Figure 2e) includes peaks at 133.6 and 132.8 eV, attributed to P–C and P–N bonds, respectively.<sup>[17,23]</sup>

The BET surface area and pore size distribution of the undoped and doped  $\text{g-C}_3\text{N}_4$  samples were determined from their  $\text{N}_2$  adsorption/desorption isotherms. In general, a high surface area can provide more active sites for the reactants, resulting in the high efficiency of the catalytic process. As can be seen from the data reported in Figure 3, the curves obtained for the OBCN, SBCN, and PBCN samples are type IV isotherms with H3 hysteresis loops. These curves are characteristic of mesoporous materials, and they stem from the difference in the curvatures of the meniscus during adsorption and desorption with a capillary condensation. The pore radius ranges between (1.5 and 4.5 nm), which confirms the presence of mesopore in the structure. The values for the BET surface area of BCN, OBCN, SBCN, and PBCN were calculated to be 11, 11, 46.9, and 38  $\text{m}^2/\text{g}$ , respectively. As presented in our previous work, the undoped  $\text{g-C}_3\text{N}_4$  has shown a similar

adsorption-desorption isotherm, hysteresis loop, and pore size distribution to doped  $\text{g-C}_3\text{N}_4$  and BET surface area of 10  $\text{m}^2/\text{g}$ .<sup>[11]</sup> As expected, BCN and OBCN have similar surface areas. Indeed, the surface area of SBCN and PBCN was manifold higher than that of the non-doped catalyst (BCN). Hence a superior catalytic performance could be expected for the SBCN and PBCN compared to BCN and OBCN due to the availability of active sites for substrate adsorption and photoreaction. The Scanning electron microscopy image of the SBCN sample is reported in Figure 3d. It shows that the sulfur-doped  $\text{g-C}_3\text{N}_4$  exhibits a stacked structure.

UV-vis absorption spectra were recorded to gather evidence on the optical absorption and calculate the energy bandgaps of the doped  $\text{g-C}_3\text{N}_4$ . The absorption spectra of OBCN, SBCN, and PBCN samples are reported in Figure 4a, and their Tauc plots are reported in Figure 4b. All three catalysts exhibited absorption in the visible region, and the absorption edge of OBCN was observed at around 473 nm. However, the spectra of SBCN and PBCN exhibited a blue shift for this absorption to 462 and 440 nm compared to OBCN, respectively. The energy bandgaps of the synthesized catalysts were calculated from their respective Tauc plots.<sup>[11]</sup> As can be seen from Figure 4b, the energy bandgaps were 2.48, 2.53, and 2.65 eV for OBCN,

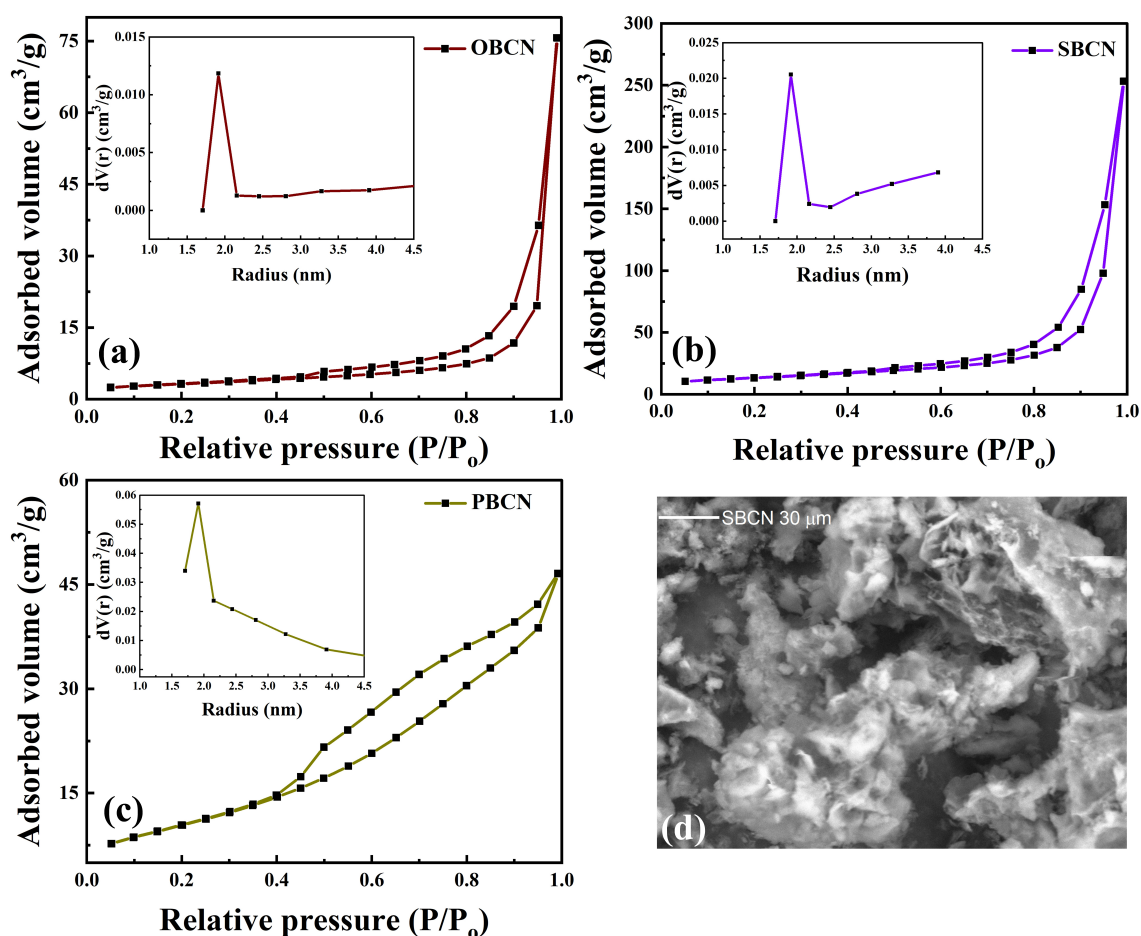


Figure 3. BET surface area and particle size distribution (shown in inset) of (a) OBCN, (b) SBCN, and (c) PBCN; (d) SEM image of the SBCN catalyst.



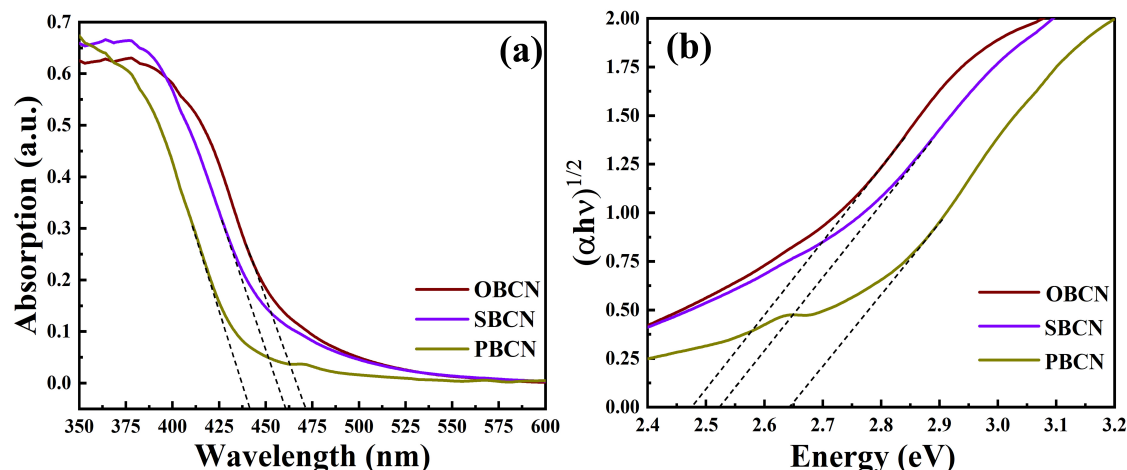


Figure 4. (a) UV-vis absorption spectra and (b) Tauc plots of OBCN, SBCN, and PBCN.

SBCN, and PBCN, respectively. In our previous published study, the bandgap of undoped bulk  $g\text{-C}_3\text{N}_4$  was determined to have a value of 2.58 eV.<sup>[11]</sup> The narrow bandgap of OBCN and SBCN compared to bulk  $g\text{-C}_3\text{N}_4$  can be ascribed to the incident light reflections in the structure, which increase the effective path length for light absorption. Meanwhile, a small amount of S and O can affect the electronic structure of  $g\text{-C}_3\text{N}_4$  to narrow the bandgap.<sup>[24]</sup> In the case of PBCN, the bandgap is wider than undoped bulk  $g\text{-C}_3\text{N}_4$  because of the high amount of P present in the structure. A large amount of impurity present in the structure can affect the electronic structure of the catalyst in such a way that it shows a blue shift and a large bandgap.<sup>[25]</sup> The  $\text{H}_3\text{PO}_4$  in melamine does not undergo complete decomposition during the heating and sublimation of melamine, so a large amount of P is present in the structure of the catalyst.<sup>[17,26]</sup>

#### Adsorption and photocatalytic performance of the catalysts

As described in the experimental section, the hormone adsorption experiments were performed in the dark. The results of the kinetics study of  $17\beta$ -estradiol adsorption are reported in Figure 5. All three photocatalysts, OBCN, SBCN, and PBCN, exhibited similar adsorption patterns; for simplicity, only the data collected for SBCN are reported here as a representative case for all studied catalysts. The adsorption kinetics curve of  $17\beta$ -estradiol is presented in Figure 5a. As shown in Figure 5a, predominantly adsorption took place in the first 5 min of the contact between  $17\beta$ -estradiol and the photocatalyst. After 15 min, there was only a minor change in the hormone concentration in the solution. Namely, after 60 min, 63% of the  $17\beta$ -estradiol was removed, while after 180 min, 66% (not shown in Figure 5a). The fast adsorption in the first 5 min can be associated with the hydrophobicity of  $17\beta$ -estradiol (octanol/water partitioning coefficient,  $\log K_{ow}$  of 4.01).<sup>[27]</sup>

Three different kinetic models were used to analyze the adsorption data: pseudo-first-order (Eq. (4)), pseudo-second-order (Eq. (5)), and Elovich kinetic model (Eq. (6)). A comparison

of the experimental and calculated data is presented in Figure 5 (b–d). The fitted model parameters are summarized in Table S1. The pseudo-second-order kinetic model showed the highest correlation coefficient value ( $R^2 = 0.999$ ) for the adsorption of  $17\beta$ -estradiol on SBCN, demonstrating that it is the best fitting model for this system. According to this model, the equilibrium adsorption capacity ( $q_e$ ) is  $17\beta$ -estradiol on SBCN 33.38 mg/g. Elovich's kinetic model exhibited a higher  $R^2$  (0.904) value than the pseudo-first-order (0.471) model.<sup>[27d]</sup>

The photocatalytic performance of synthesized photocatalysts for hormone degradation was investigated. First, a photolysis experiment was conducted without a catalyst (Figure 6a) to determine whether these hormones undergo self-degradation in visible light. There was almost negligible degradation during the photolysis reaction. All other experiments were performed in the presence of the catalysts. The homogeneous dispersion of the catalyst was ensured by sonicating the reaction mixture (i.e., the mixture comprising the water solution of the hormones and the catalyst) and by stirring it for 15 min (an optimal time chosen after initial adsorption experiments) in the dark. The reaction time starts as soon as the light is turned on; only an adsorption process takes place up to that moment.

As shown from the data reported in Figure 6a, the sulfur-doped SBCN sample demonstrated the highest adsorption and photodegradation with almost complete removal of  $17\beta$ -estradiol in 45 min; over the same period, 86% removal was achieved with BCN, 88% with OBCN, and 64% with PBCN. From this amount, 63%, 59%, 57%, and 55% of  $17\beta$ -estradiol were removed by adsorption on SBCN, BCN, OBCN, and PBCN, respectively. For BCN and OBCN, a relatively lower surface area limits the adsorption and, subsequently, the photodegradation of the  $17\beta$ -estradiol. BCN and OBCN have shown almost the same activity because of the similar nature confirmed by XRD, BET, and FTIR. Notably, PBCN exhibited negligible photodegradation, and with this catalyst, the  $17\beta$ -estradiol was removed primarily by adsorption. The observed poor perform-

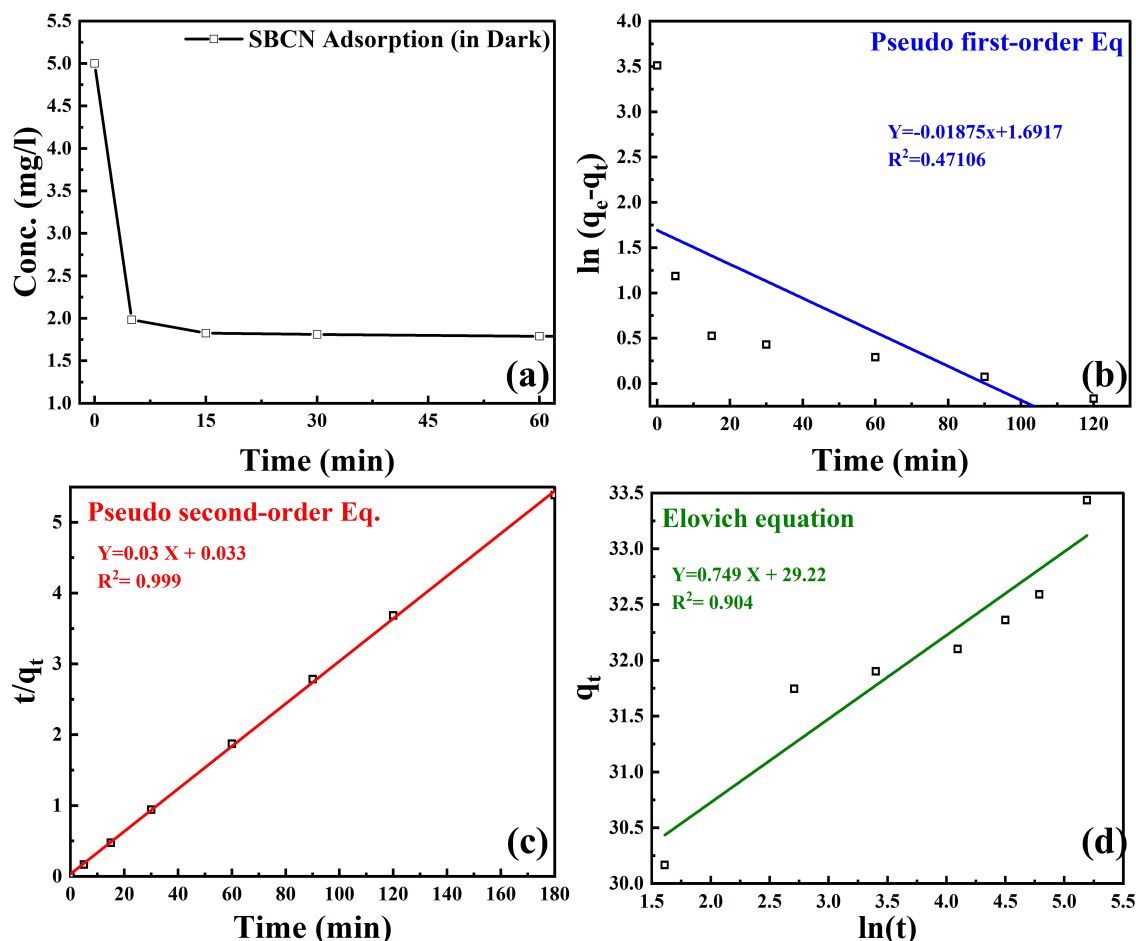


**Figure 5.** (a) Adsorption kinetics of 17β-estradiol with 0.1 g/L SBCN and 5 mg/L pollutant concentration; (b) pseudo-first-order model, (c) pseudo-second-order model, and (d) Elovich model, pH 7, temperature 25 °C.

ance of PBCN may have to do with the fact that P atoms had replaced the structural C and N atoms, and there is a large amount of residual  $\text{PO}_4^{3-}$  species in the catalyst, which suppressed catalytic activity.

Different amounts of catalyst were used further to investigate the kinetics of the photocatalytic degradation reaction. For this study, SBCN was selected as the best performing catalyst, and its concentration in a 17β-estradiol aqueous solution varied between 0.05 and 0.2 g/L. The 17β-estradiol removal curves are presented in Figure 6b. The photocatalytic degradation efficiency increases with the amount of catalyst because the number of active sites increases with the increase of the catalyst.<sup>[11]</sup> However, it should be noted that complete 17β-estradiol removal was achieved in 45 min with 0.1 and 0.2 g/L of SBCN catalyst.

In the following, adsorption followed by photodegradation was also carried out for 17α-ethinylestradiol with the 0.1 g/L SBCN catalyst. As can be seen from Figure 6c, the 17α-ethinylestradiol was also entirely degraded and removed from water in 45 min. Notably, the photodegradation of 17α-ethinylestradiol was even faster than that of 17β-estradiol. This observation is due to the presence of unsaturated triple bonds

in 17α-ethinylestradiol, which readily undergo oxidation to produce less harmful products. This study can provide an initial base, but optimizing the amount of catalyst should be performed to save the cost for other hormonal pollutants selected. The chemical structures of both compounds are reported in Table S2.

The photodegradation curves reported in Figure 6 were well-fitted by an exponential decay model, and by fitting the said curves with this model, the reaction rate constant ( $k$ ) could be calculated utilizing the following equation (1):

$$\frac{C}{C_0} = e^{-kt} \quad (1)$$

where  $C$  is the concentration of 17β-estradiol at irradiation time  $t$ ,  $C_0$  is the 17β-estradiol concentration after adsorption in this case, i.e., at the beginning of the photocatalytic degradation reaction, and  $k$  is the rate constant. The rate constant  $k$  for SBCN, OBCN, and PBCN were 0.139, 0.046, and 0.008  $\text{min}^{-1}$ , respectively. In detail, the decomposition of  $\text{SO}_4^{2-}$  during the heat treatment of melamine contributed to SBCN acquiring a porous structure, which benefited substrate adsorption and

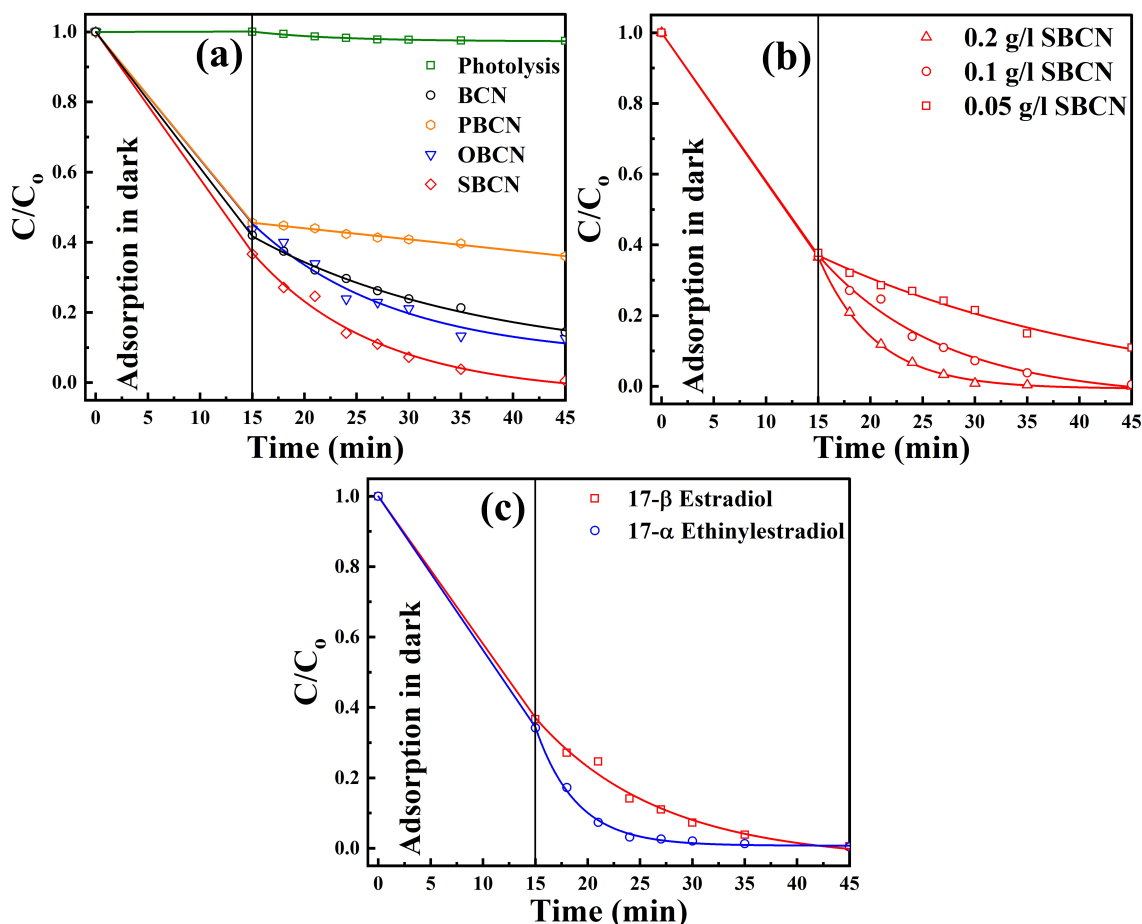


**Figure 6.** Photocatalytic degradation curves of (a) 17β-estradiol with doped  $g-C_3N_4$  catalysts with a catalyst concentration of 0.1 g/L; (b) 17β-estradiol using different concentrations of SBCN catalyst, and (c) 17β-estradiol and 17α-ethinylestradiol at 0.1 g/l SBCN.

increased the accessibility of the active catalytic sites. The photodegradation curves for the different amounts of best-performing SBCN reported in Figure 6b fit the exponential decay model. The values for the rate constant  $k$  for the degradation reactions whereby the SBCN concentrations were 0.2, 0.1, and 0.05 g/L were 0.24, 0.139, and 0.042  $\text{min}^{-1}$ , respectively.

The re-usability of SBCN was demonstrated by performing two cycles of hormone degradation after subjecting the catalyst to thorough washing and drying at 120 °C for 12 h. The degradation efficiency of the catalyst remained unchanged, and the material remained stable for at least two cycles (Supplementary Figure S2).

### Photocatalytic degradation mechanism

The typical mechanism is given in equations (2)–(8). These photo-induced charge carriers and radicals eventually lead to the degradation of pollutants by the reduction and oxidation processes. The primary intermediates and products of E2 were analyzed and identified by LC/MS. The identification results are presented in Table 1. The SBCN can generate electrons  $e^-$  and

holes  $h^+$  in the conduction and valence band when irradiated with light to react with the adsorbed hormones on the surface of the SBCN catalyst. The generated holes can directly oxidize water or hydroxide ions to hydroxyl radical ( $\bullet OH$ ). The oxygen molecules present in the system can accept the electron to produce the superoxide radical ( $\bullet O_2^-$ ). These superoxide radicals can also produce hydroxyl radicals ( $\bullet OH$ ). The generated radicals and holes react with the pollutants to produce intermediates and products.<sup>[11,28]</sup> The presence of these ROS, e.g., hydrogen peroxide using  $g-C_3N_4$ , was previously confirmed.<sup>[28,29]</sup>

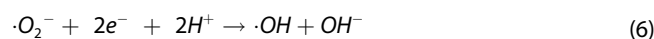
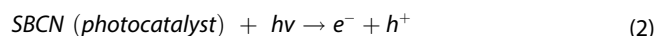


Table 1. Degradation products of E2.

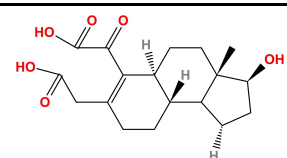
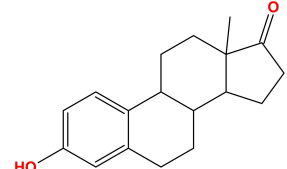
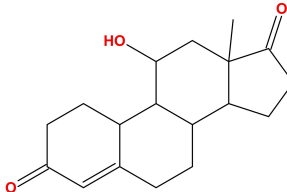
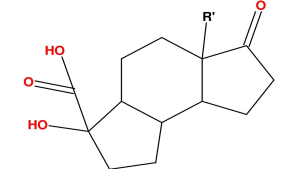
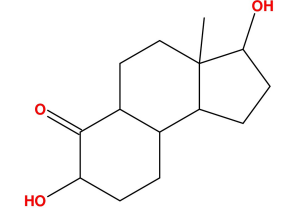
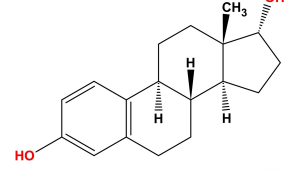
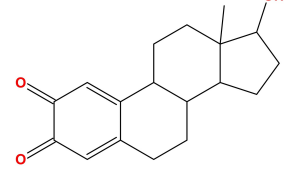
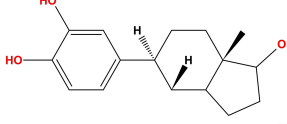
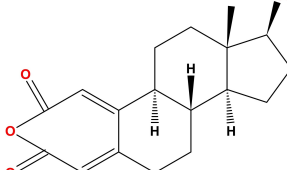
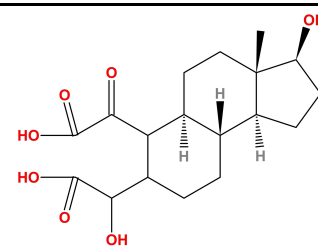
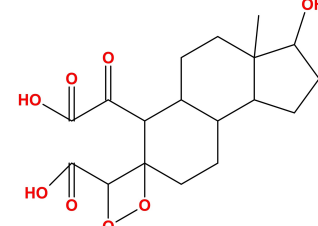
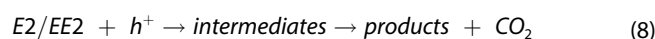
No	Molecular Formula	<i>m/z</i>	Probable structure	Ref
1	C <sub>18</sub> H <sub>24</sub> O <sub>6</sub>	335.11		[28a]
2	C <sub>18</sub> H <sub>22</sub> O <sub>2</sub>	269.14		[30]
3	C <sub>18</sub> H <sub>26</sub> O <sub>3</sub>	288.70		[30]
4	C <sub>14</sub> H <sub>20</sub> O <sub>4</sub>	251.17		[31]
5	C <sub>14</sub> H <sub>22</sub> O <sub>3</sub>	236.91		[30]
6	C <sub>18</sub> H <sub>24</sub> O <sub>2</sub>	271.15		[32]
7	C <sub>18</sub> H <sub>22</sub> O <sub>3</sub>	285.14		[30]
8	C <sub>18</sub> H <sub>24</sub> O <sub>3</sub>	287.13		[28a]
9	C <sub>18</sub> H <sub>22</sub> O <sub>4</sub>	301.16		[32]

Table 1. continued

No	Molecular Formula	<i>m/z</i>	Probable structure	Ref
10	C <sub>18</sub> H <sub>24</sub> O <sub>7</sub>	352.96		[32]
11	C <sub>18</sub> H <sub>24</sub> O <sub>8</sub>	365.69		[30]



The degradation products formed during the photocatalytic experiments determined using the LC-MS method described in the materials and method section are listed in Table 1

## Conclusion

In summary, undoped and nonmetal sulfur, oxygen, and phosphorous doped g-C<sub>3</sub>N<sub>4</sub> (BCN, SBCN, OBCN, and PBCN) were successfully synthesized from untreated and acid-treated melamine. The photocatalytic performance of obtained catalysts was tested to degrade two hormones, namely 17β-estradiol and 17α-ethinylestradiol, under visible light irradiation. PXRD, FTIR, and XPS analyses confirmed the phase and chemical structures of g-C<sub>3</sub>N<sub>4</sub> and its derivatives obtained by doping g-C<sub>3</sub>N<sub>4</sub> with nonmetals. Among the synthesized g-C<sub>3</sub>N<sub>4</sub> derivatives, sulfur-doped g-C<sub>3</sub>N<sub>4</sub> (SBCN) exhibited the highest photocatalytic activity toward the studied hormones due to its higher BET surface area and narrower energy bandgap than the other three catalysts. The hormone adsorption on SBCN was quick due to the hydrophobic nature of these hormones. The adsorption was followed by photodegradation under visible light (430 nm) irradiation. Complete removal of 17β-estradiol was achieved in 45 min, and of 17α-ethinylestradiol was achieved in 30 min. Three kinetic adsorption models were used to fit the experimental data, and the pseudo-second-order model was observed to best represent the adsorption of 17β-estradiol onto SBCN. The proposed mechanism of the ROS generation and intermediate products from pollutant photodegradation are presented. The nonmetal doping of g-C<sub>3</sub>N<sub>4</sub> via acid-treated melamine modified its energy bandgap and helped increase the surface area. As a result, it enhanced the



photocatalytic activity to degrade the endocrine-disrupting compounds from the water.

## Experimental Section

### Reagents and chemicals

Melamine (C<sub>3</sub>H<sub>6</sub>N<sub>6</sub>, 99%) (Alfa Aesar), sulfuric acid (H<sub>2</sub>SO<sub>4</sub>, 96%) (VWR Chemicals), orthophosphoric acid (H<sub>3</sub>PO<sub>4</sub>, 85%) (VWR Chemicals), acetic acid (CH<sub>3</sub>COOH), (VWR Chemicals), acetonitrile (C<sub>2</sub>H<sub>3</sub>N, 99.99%) (Sigma Life Science), 17β-estradiol (C<sub>18</sub>H<sub>24</sub>O<sub>2</sub>, 99%) (Sigma Life Science), 17α-ethinylestradiol (C<sub>20</sub>H<sub>24</sub>O<sub>2</sub>, 99%) (Sigma Life Science), methanol (Sigma Aldrich) and ultrapure water for HPLC (Sigma Aldrich) were used as received without pre-treatment.

### Synthesis of g-C<sub>3</sub>N<sub>4</sub>

g-C<sub>3</sub>N<sub>4</sub> was prepared using the published procedure involving the thermal decomposition of melamine.<sup>[12]</sup> Specifically, a muffle furnace kept under a static air atmosphere was used to synthesize g-C<sub>3</sub>N<sub>4</sub> from melamine (5 g) in a closed crucible. A 2 °C/min heating gradient was set in a two-step heating process until 450 °C was reached; this temperature was then maintained for 2 h. Subsequently, 550 °C was set as the final temperature, with a heating ramp of 2 °C/min; the muffle furnace was kept at the mentioned temperature for 4 h. A roughly 50% yield of bulk g-C<sub>3</sub>N<sub>4</sub> was obtained by conducting this process. The isolated material was allowed to cool down to room temperature naturally; it was then weighed and ground up using a mortar and pestle. The as-prepared g-C<sub>3</sub>N<sub>4</sub> was then washed and filtered; it was subsequently dried overnight in an oven at 80 °C.

### Synthesis of doped g-C<sub>3</sub>N<sub>4</sub>

The non-metallic doped g-C<sub>3</sub>N<sub>4</sub> was prepared by treating melamine with acetic acid, sulfuric acid, and phosphoric acid to achieve oxygen, sulfur, and phosphorous doping. In detail, melamine was mixed with a 2 M solution of the relevant acid. The mixture thus obtained was stirred for 2 h; the mixture was then centrifuged, washed, and filtered to obtain the relevant doped melamine sample. The said sample was thus used to prepare the relevant doped g-C<sub>3</sub>N<sub>4</sub> material via the same procedure implemented to prepare undoped g-C<sub>3</sub>N<sub>4</sub>. The undoped bulk sample was named BCN, and the doped bulk samples were named OBCN, SBCN, and PBCN, which stood for oxygen, sulfur, and phosphorus-doped g-C<sub>3</sub>N<sub>4</sub>, respectively.

### Characterizations of the catalyst

The N<sub>2</sub> sorption isotherms recorded to determine the values of the samples' Brunauer–Emmett–Teller (BET) surface area, pore size distribution, and pore volume were determined using an autosorb <sup>®</sup>iQ-MP/XR (Nova 4200e), Quantachrome instrument (Germany). Sample degassing was performed at 120 °C for 3 h before the analysis. The surface area of the catalyst was calculated from the N<sub>2</sub> sorption isotherms obtained at −196 °C. The Barrett–Joyner–Halenda (BJH) method determined the samples' pore size distribution. A Bruker D8 instrument with Cu Kα radiation (1.54 Å) (40 kV, 40 mA), a spin speed of 40 rpm in the range between 3° and 35°, and a step size of 0.01° was employed to study the crystalline phases of the synthesized catalysts. A Spectrum, Two FTIR Spectrometer (PerkinElmer, Switzerland) with a universal ATR

(UATR Two) cell equipped with a ZnSe single crystal, was used to collect the Fourier-transform infrared (FTIR) spectra of the samples in the 400–4000 cm<sup>−1</sup> wavenumber range. The FTIR spectral measurements were conducted at 4 cm<sup>−1</sup> and 60 scans. X-ray photoelectron spectroscopy (XPS) showed the samples' surface chemical analysis. A Kratos Axis Ultra DLD spectrometer with a monochromated Al Kα X-ray source operating at 168 W (12 mA × 14 kV) was used to collect the data. Step sizes of 1 and 0.1 eV were used for the survey spectra, and high-resolution scans were recorded with pass energies of 160 and 20 eV, respectively. Ultraviolet-visible (UV-vis) absorption spectra were recorded using a UV-3600 Plus spectrometer (Shimadzu, Kyoto, Japan) with medium scan speed using a 20-slit width with three external detectors in the 200–800 nm wavelength range.

### Hormone adsorption and photocatalytic degradation

This study performed two types of experiments: adsorption experiments in the absence of light and photocatalytic degradation in the presence of light. The experiments were carried out in a jacketed glass reactor with a maximum working capacity of 120 mL and placed in a safety cabinet (Peschl Ultraviolet GmbH, Mainz, Germany). SBCN experiments were performed in duplicates to ensure the reproducibility of the results. The irradiation for photocatalytic experiments was done using a custom-made immersion LED lamp comprising five individual LEDs (10 W) with a maximum emission of 430 nm. The photocatalytic reactor setup is shown in Figure S3.

First, only adsorption experiments in the absence of light were performed to evaluate the removal of the hormone by adsorption. The catalyst was suspended in a 5 mg/L hormone aqueous solution prepared from 1000 mg/L stock solution in methanol and stirred for 180 min. Samples were taken at regular time intervals and analyzed with the HPLC. For the adsorption/photocatalytic degradation experiments, the photocatalyst was added to a hormone aqueous solution in the reactor. The reactor was sonicated for 15 min to ensure the catalyst's homogenous dispersion in the solution. Afterward, the solution was stirred for 15 min in the dark under an airflow (50 mL/min). A sample was taken for analysis to determine the hormone concentration of the solution after the adsorption step. Next, the LED lamp was turned on, the photocatalytic reaction was started, and samples were collected at regular intervals. A photolysis experiment was conducted without a catalyst to verify the extent of self-degradation of 17β-estradiol under light irradiation.

The removal efficiency was evaluated by using equation (9):

$$\text{Total removal efficiency (\%)} = \frac{C_0 - C}{C_0} * 100 \quad (9)$$

where C<sub>0</sub> and C represent the pollutant concentrations at the beginning of the experiment (t = 0) and after a specific time interval of t, respectively.

The adsorption kinetics of 17β-estradiol was modeled using pseudo-first-order, pseudo-second-order, and Elovich kinetic models [Eq. (10)–(12)].<sup>[27d]</sup> The following equations were used to fit the adsorption data:

Pseudo-first-order model

$$\ln(q_e - q_t) = \ln q_e - k_1 t \quad (10)$$

Pseudo-second-order model

$$t/q_t = 1/k_2q_e^2 + t/q_e \quad (11)$$

Elovich equation

$$q_t = \left(1/\beta\right)\ln(\alpha\beta) + \left(1/\beta\right)\ln(t) \quad (12)$$

where  $k_1$  and  $k_2$  are the rate constants in  $\text{min}^{-1}$  and  $q_e$  and  $q_t$  are adsorption capacities at equilibrium and at time  $t$  in Eqs. (10) and (11), respectively. Notably, the constants  $\alpha$  and  $\beta$  in Eq. (12) represent the initial adsorption rate ( $\text{mg/g}\cdot\text{min}$ ) and the extent of surface coverage of the adsorbent and the activation energy, respectively.

### Analytical methods

The concentrations of  $17\beta$ -estradiol and  $17\alpha$ -ethinylestradiol were determined using a Prominence HPLC system (Shimadzu, Japan) comprising a binary pump (LC-20AB), a SIL-20 A autosampler, a DGU-20 A3 degasser, an SPD-M20 A diode-array detector and a single quadrupole MS (LCMS-2020). The analysis was conducted employing a Phenomenex (C18, 150 mm  $\times$  4.6 mm, 3  $\mu\text{m}$ ) column at a fixed flow rate of 0.8 mL/min, using 40% acetonitrile in water as the eluent; the run time was 10 min (sample injection volume 10  $\mu\text{L}$ ; detection wavelength 205 nm). The following MS conditions were used: dual ion source (DUIS),  $m/z$  range 50–500, negative ionization mode, nebulizing gas flow 2 L  $\text{min}^{-1}$ , drying gas flow 15 L  $\text{min}^{-1}$ , DL temperature 300  $^\circ\text{C}$ , heat block temperature 500  $^\circ\text{C}$ .

### Supporting Information Summary

Details of the characterization results (Figure S1), stability result (Figure S2), Details of the reactor (Figure S3), fitting data for the adsorption models (Table S1), and chemical structure of E2 and EE2 (Table S2) are provided in supporting information.

### Acknowledgements

Adeem Ghaffar Rana thanks the DAAD, Germany, and Higher Education Commission (HEC), Pakistan. Open Access funding enabled and organized by Projekt DEAL.

### Conflict of Interest

The authors declare no conflict of interest.

### Data Availability Statement

The data that support the findings of this study are available in the supplementary material of this article.

**Keywords:** graphitic carbon nitride · hormones · photocatalysis · water treatment ·  $17\beta$ -estradiol ·  $17\alpha$ -ethinylestradiol

- [1] M. J. Arlos, R. Liang, M. M. Hatat-Fraile, L. M. Bragg, N. Y. Zhou, M. R. Servos, S. A. Andrews, *J. Hazard. Mater.* **2016**, *318*, 541–550.
- [2] L. Li, Y. Long, Y. Chen, S. Wang, L. Wang, S. Zhang, F. Jiang, *Solid State Sci.* **2018**, *83*, 143–151.
- [3] A. R. Upreti, Y. Li, N. Khadgi, S. Naraginti, C. Zhang, *RSC Adv.* **2016**, *6*, 32761–32769.
- [4] V. M. Mboula, V. Héquet, Y. Andrès, Y. Gru, R. Colin, J. M. Doña-Rodríguez, L. M. Pastrana-Martínez, A. M. T. Silva, M. Leleu, A. J. Tindall, S. Mateos, P. Falaras, *Appl. Catal. B* **2015**, *162*, 437–444.
- [5] N. G. Menon, L. George, S. S. V. Tatiparti, S. Mukherji, *J. Environ. Manage.* **2021**, *288*, 112340.
- [6] L. Orozco-Hernandez, L. M. Gomez-Olivan, A. Elizalde-Velazquez, R. Natividad, L. Fabian-Castono, N. SanJuan-Reyes, *Sci. Total Environ.* **2019**, *669*, 955–963.
- [7] J. Mai, W. Sun, L. Xiong, Y. Liu, J. Ni, *Chemosphere* **2008**, *73*, 600–606.
- [8] a) R. Andreozzi, V. Caprio, A. Insola, R. Marotta, *Catal. Today* **1999**, *53*, 51–59; b) A. G. Rana, W. Ahmad, A. Al-Matar, R. Shawabkeh, Z. Aslam, *Environ. Technol.* **2017**, *38*, 1085–1092.
- [9] J. A. Garrido-Cardenas, B. Esteban-Garcia, A. Aguera, J. A. Sanchez-Perez, F. Manzano-Agugliaro, *Int. J. Environ. Res. Public Health* **2019**, *17*, 21–39.
- [10] H. Sudrajat, *J. Solid State Chem.* **2018**, *257*, 26–33.
- [11] A. G. Rana, M. Tasbihi, M. Schwarze, M. Minceva, *Catalysts* **2021**, *11*, 662–679.
- [12] A. G. Rana, M. Minceva, *Catalysts* **2021**, *11*, 898–913.
- [13] S. Guo, Y. Tang, Y. Xie, C. Tian, Q. Feng, W. Zhou, B. Jiang, *Appl. Catal. B* **2017**, *218*, 664–671.
- [14] L. Zhang, X. Chen, J. Guan, Y. Jiang, T. Hou, X. Mu, *Mater. Res. Bull.* **2013**, *48*, 3485–3491.
- [15] K. Wang, Q. Li, B. Liu, B. Cheng, W. Ho, J. Yu, *Appl. Catal. B* **2015**, *176–177*, 44–52.
- [16] C.-Y. Kuo, C.-H. Wu, J.-T. Wu, Y.-R. Chen, *React. Kinet. Mech. Catal.* **2014**, *114*, 753–766.
- [17] Y. Zhao, J. Liu, C. Wang, X. Zhang, C. Chen, X. Zhao, J. Li, H. Jin, *J. Power Sources* **2019**, *424*, 176–183.
- [18] a) M. J. Lima, A. M. T. Silva, C. G. Silva, J. L. Faria, *J. Catal.* **2017**, *353*, 44–53; b) X. Yuan, C. Zhou, Y. Jin, Q. Jing, Y. Yang, X. Shen, Q. Tang, Y. Mu, A. K. Du, *J. Colloid Interface Sci.* **2016**, *468*, 211–219; c) M. J. Muñoz-Batista, D. Rodríguez-Padrón, A. R. Puente-Santiago, A. Kubacka, R. Luque, M. Fernández-García, *ChemPhotoChem* **2018**, *2*, 870–877.
- [19] a) M. Arif, G. Yasin, M. Shakeel, X. Fang, R. Gao, S. Ji, D. Yan, *Chem. Asian J.* **2018**, *13*, 1045–1052; b) Y. O. Ibrahim, A. Hezam, T. F. Qahtan, A. H. Al-Aswad, M. A. Gondal, Q. A. Drmash, *Appl. Surf. Sci.* **2020**, *534*, 86–95.
- [20] Z. Liu, X. Zhang, Z. Jiang, H.-S. Chen, P. Yang, *Int. J. Hydrogen Energy* **2019**, *44*, 20042–20055.
- [21] a) L. G. Devi, R. Kavitha, *Mater. Chem. Phys.* **2014**, *143*, 1300–1308; b) H. Xie, Y. Zheng, X. Guo, Y. Liu, Z. Zhang, J. Zhao, W. Zhang, Y. Wang, Y. Huang, *ACS Sustainable Chem. Eng.* **2021**, *9*, 6788–6798; c) D. A. Tran, C. T. Nguyen Pham, T. Nguyen Ngoc, H. Nguyen Phi, Q. T. Hoai Ta, D. H. Truong, V. T. Nguyen, H. H. Luc, L. T. Nguyen, N. N. Dao, S. J. Kim, V. Vo, *J. Phys. Chem. Solids* **2021**, *151*, 26–35; d) F. Wei, Y. Liu, H. Zhao, X. Ren, J. Liu, T. Hasan, L. Chen, Y. Li, B. L. Su, *Nanoscale* **2018**, *10*, 4515–4522; e) Y. Zhang, Z. Chen, J. Li, Z. Lu, X. Wang, *J. Energy Chem.* **2021**, *54*, 36–44.
- [22] a) H. Yan, Y. Chen, S. Xu, *Int. J. Hydrogen Energy* **2012**, *37*, 125–133; b) S. Cao, B. Fan, Y. Feng, H. Chen, F. Jiang, X. Wang, *Chem. Eng. J.* **2018**, *353*, 147–156; c) K. Guan, J. Li, W. Lei, H. Wang, Z. Tong, Q. Jia, H. Zhang, S. Zhang, *J. Mater.* **2021**, *7*, 1131–1142; d) Z. Zhu, Z. Liu, X. Tang, K. Reeti, P. Huo, J. W.-C. Wong, J. Zhao, *Catal. Sci. Technol.* **2021**, *11*, 1725–1736; e) X. Xiao, Y. Wang, Q. Bo, X. Xu, D. Zhang, *Dalton Trans.* **2020**, *49*, 8041–8050; f) N. D. Shcherban, S. M. Filonenko, M. L. Ovcharov, A. M. Mishura, M. A. Skoryk, A. Aho, D. Y. Murzin, *ChemistrySelect* **2016**, *1*, 4987–4993; g) F. Zhao, H. Cheng, Y. Hu, L. Song, Z. Zhang, L. Jiang, L. Qu, *Sci. Rep.* **2014**, *4*, 5882; h) D. Long, L. Wang, H. Cai, X. Rao, Y. Zhang, *Catal. Lett.* **2020**, *150*, 2487–2496.
- [23] a) D. Vashisht, E. Sharma, M. Kaur, A. Vashisht, S. K. Mehta, K. Singh, *Spectrochim. Acta Part A* **2020**, *228*, 117773; b) X. Qin, L. Jing, G. Tian, Y. Qu, Y. Feng, *J. Hazard. Mater.* **2009**, *172*, 1168–1174.
- [24] Q. Fan, J. Liu, Y. Yu, S. Zuo, B. Li, *Appl. Surf. Sci.* **2017**, *391*, 360–368.
- [25] D. Mocatta, G. Cohen, J. Schattner, O. Millo, E. Rabani, U. Banin, *Science* **2011**, *332*, 77–81.
- [26] L. Jiang, X. Yuan, G. Zeng, X. Chen, Z. Wu, J. Liang, J. Zhang, H. Wang, H. Wang, *ACS Sustainable Chem. Eng.* **2017**, *5*, 5831–5841.

- [27] a) E. Nazari, F. Suja, *Rev. Environ. Health* **2016**, *31*, 465–491; b) A. M. E. Khalil, F. A. Memon, T. A. Tabish, D. Salmon, S. Zhang, D. Butler, *Chem. Eng. J.* **2020**, *398*, 461–470; c) J. Ferandin Honorio, M. T. Veit, P. Y. R. Suzaki, P. F. Coldebella, E. Sloboda Rigobello, C. R. G. Tavares, *Environ. Technol.* **2020**, *41*, 1075–1092; d) M. Z. Hussain, Z. Yang, A. M. E. Khalil, S. Hussain, S. U. Awan, Q. Jia, R. A. Fischer, Y. Zhu, Y. Xia, *J. Mater. Sci. Technol.* **2022**, *101*, 49–59.
- [28] a) T. Huang, B. Pan, H. Ji, W. Liu, *Water* **2020**, *12*; b) Y. Long, D. Huang, L. Luo, L. Li, L. Wang, S. Zhang, F. Jiang, *Res. Chem. Intermed.* **2018**, *44*, 7117–7133; c) A. Torres-Pinto, M. J. Sampaio, C. G. Silva, J. L. Faria, A. M. T. Silva, *Appl. Catal. B* **2019**, *252*, 128–137.
- [29] a) S. D. Rojas, N. Espinoza-Villalobos, R. Salazar, N. Escalona, D. Contreras, V. Melin, M. A. Laguna-Bercero, M. Sánchez-Arenillas, E. Vergara, L. Caceres-Jensen, J. Rodriguez-Becerra, L. Barrientos, *J. Photochem. Photobiol. A* **2021**, *421*, 45–56; b) J. Liu, C. Xiong, S. Jiang, X. Wu, S. Song, *Appl. Catal. B* **2019**, *249*, 282–291; c) H. Tan, P. Kong, R. Zhang, M. Gao, M. Liu, X. Gu, W. Liu, Z. Zheng, *Innovation (Camb)* **2021**, *2*, 215–227.
- [30] Y. Liu, H. Guo, Y. Zhang, W. Tang, *RSC Adv.* **2016**, *6*, 79910–79919.
- [31] A. Kumar, A. Kumar, G. Sharma, M. Naushad, R. C. Veses, A. A. Ghfar, F. J. Stadler, M. R. Khan, *New J. Chem.* **2017**, *41*, 10208–10224.
- [32] Y. Chen, L. Sun, Z. Yu, L. Wang, G. Xiang, S. Wan, *Sep. Purif. Technol.* **2015**, *152*, 46–54.

Submitted: May 16, 2022

Accepted: August 4, 2022